Z-Shaped MEMS Thermal Actuators: Piezoresistive Self-Sensing and Preliminary Results for Feedback Control

Jing Ouyang and Yong Zhu

***Abstract*—Feedback control of microactuators holds potential to significantly improve their performance and reliability. A critical step to realize the feedback control of microactuators is feedback sensing. In this paper, we report the feasibility of using a Z-shaped thermal actuator (ZTA) as a simultaneous force or displacement sensor. An *in situ* scanning electron microscope nanomanipulation process is used to characterize the piezoresistive response of ZTAs, which shows that ZTAs can be used as piezoresistive sensors. The experimental results agree very well with multiphysics (electric–thermal-structural-piezoresistive) simulations. A new feedback scheme is further explored, where the ZTA is treated as a two-input (applied current and external force) and two-output (displacement and electric resistance) system. Based on the calibrated relationships between the inputs and the outputs, a feedback system is developed, which can simultaneously sense the external force and generate updated current to actuate the ZTA to the desired position. We demonstrate preliminary results of this feedback control by holding the ZTA at a constant position under various external forces. The device and method presented in this paper are valuable for a range of microelectromechanical systems applications, including on-chip nanoscale mechanical testing and nanopositioning. [2011-0282]**

***Index Terms*—Feedback control, nanomechanical testing, piezoresistivity, self-sensing, thermal actuator, Z-shaped.**

I. Introduction

In THE field of microelectromechanical systems (MEMS), thermal actuators have emerged as compact, stable, and high-force actuation apparatuses [1]–[4]. Thermal actuators in a variety of configurations have been exploited for achieving in-plane motion. One is the pseudobimorph (U-shaped) thermal actuator [1], [5], which employs asymmetrical thermal beams with different cross-sectional areas. The locus of motion is an arc. The other is the bent-beam (V-shaped) thermal actuator [3], [4], [6] utilizing thermal expansion of symmetric slanted beams to generate rectilinear displacement of the central shuttle. In addition, we have recently introduced a new Z-shaped thermal actuator (ZTA), which is similar to the V-shaped one except using Z-shaped beams instead of V-shaped beams [2]. As will be discussed later, the ZTA offers several complementary features to the V-shaped one.

Thermal actuators have been employed in a broad range of applications, including on-chip nanoscale material testing system [6]–[8], linear and rotary microengines [9], nanopositioner [10], and bistable mechanism [11]. Closed-loop feedback control of thermal actuators is useful in improving the system performance and reliability for many of these applications. One of the major challenges for feedback control of MEMS devices is the feedback sensor [12], [13]. For in-plane motion, optical microscopes and scanning electron microscopes (SEMs) are often used to measure the displacement. Although these techniques are good for calibrating displacements of MEMS devices, they cannot be used for closed-loop control or measurement during operation. On-chip MEMS position sensors commonly exploit capacitive and piezoresistive effects. Capacitive sensors are widely used in surface micromachined devices and have been successfully used for feedback control, e.g., the accelerometers from Analog Devices. However, sophisticated circuitry and techniques to eliminate the influence of parasitic capacitance, stray capacitance, etc., are required [12], [14], [15]. Piezoresistive sensing has been recently demonstrated for detecting in-plane displacement. In such devices, typically, the actuation and piezoresistive sensing are implemented through separate physical structures [13], [16]. Thus, the additional sensing structure increases the overall size of the device and also adds to the moving mass of the system, which results in a shift of the resonant frequency. It is therefore of interest to use the same actuator structure, simultaneously for both actuation and sensing.

The other challenge is the feedback control. Proportional–integral-derivative (PID) controller is perhaps the most widely used feedback controller and has been successfully employed in many microdevices [13], [17]. A notable limitation with PID controllers alone is that control performance may be impaired because the differentiator amplifies high-frequency noises, particularly in a noisy environment. In this paper, we explore a new approach to realize the feedback by establishing a continuous formula between inputs and outputs through data fitting. Our approach could be combined with a PID controller to further improve the feedback response.

In this paper, we report the feasibility of using an existing ZTA as a simultaneous force sensor. We characterized the piezoresistive response of ZTAs by *in situ* SEM

Manuscript received September 21, 2011; revised December 8, 2011; accepted January 26, 2012. Date of publication March 23, 2012; date of current version May 28, 2012. This work was supported by the National Science Foundation under Award CMMI-1030637. Subject Editor C. Ahn.

The authors are with the Department of Mechanical and Aerospace Engineering, North Carolina State University, Raleigh, NC 27695 USA (e-mail: jouyang@ncsu.edu; yong_zhu@ncsu.edu).

Color versions of one or more of the figures in this paper are available online at http://ieeexplore.ieee.org.

Digital Object Identifier 10.1109/JMEMS.2012.2189361

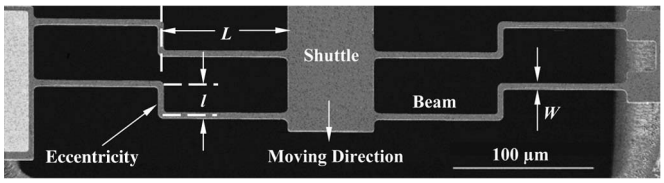

Fig. 1. SEM image of a ZTA. The black area is the etched hole underneath the actuator.

nanomanipulation and demonstrated ZTAs as viable piezoresistive sensors. We found that their sensitivity depends on the applied current and their resolution is limited by the noise. We further treated the ZTA as a two-input (applied current and external force) and two-output (displacement and electric resistance) system. Based on the calibrated relationships between the inputs and the outputs, we developed a feedback system that can simultaneously sense the external force and generate updated current to actuate the ZTA to the desired position. We demonstrated the performance of this feedback control by holding the ZTA at a constant position under various external forces.

II. Device Description

The recently developed ZTA consists of a suspended shuttle supported by two symmetric arrays of thin beams that are anchored to the substrate [2], as shown in Fig. 1. These beams are Z shaped, kinked in the direction of the desired displacement. When a voltage is applied across the actuator, the Joule heating effect generates heat and temperature rise in the beams. As a result, the beams expand. Due to the short vertical beam in the Z-shape design (eccentricity as defined in Fig. 1) and the overall symmetry, the Z-shaped beam deflects toward the desired direction and hence moves the central shuttle forward [2]. The geometry of the ZTA amplifies the relatively small thermal expansion in beams to achieve relatively large displacement of the center shuttle. Fig. 2(a) shows the displacement changes as a function of applied current.

The ZTAs could be complementary to the widely used comb drives and V-shaped thermal actuators. The ZTAs share many features in common with the V-shaped ones. Essentially, Z-shaped actuators are based on beam bending, while V-shaped actuators are based on beam extension. As a result, Z-shaped actuators possess a large range of stiffness and output force that is in between those of the comb drives and V-shaped thermal actuators, thus filling the gap between these two well-established actuators. In particular, Z-shaped actuators can achieve smaller stiffness without buckling, which makes them possible to be simultaneous force sensors as to be described in the rest of this paper. More details on the features of ZTAs can be seen in [2].

The ZTAs were fabricated at MEMSCAP (Durham, NC) using the Silicon-on-Insulator Multi-User MEMS Processes [18]. The structure layer is n-type (phosphorus) doped single-crystalline silicon (SCS). The resulted piezoresistivity offers the possibility of exploiting the ZTA as a piezoresistive sensor.

III. Piezoresistivity Measurement and Simulation

Two effects can lead to resistance change in a ZTA, namely, temperature change and piezoresistivity [16]. The resistivity

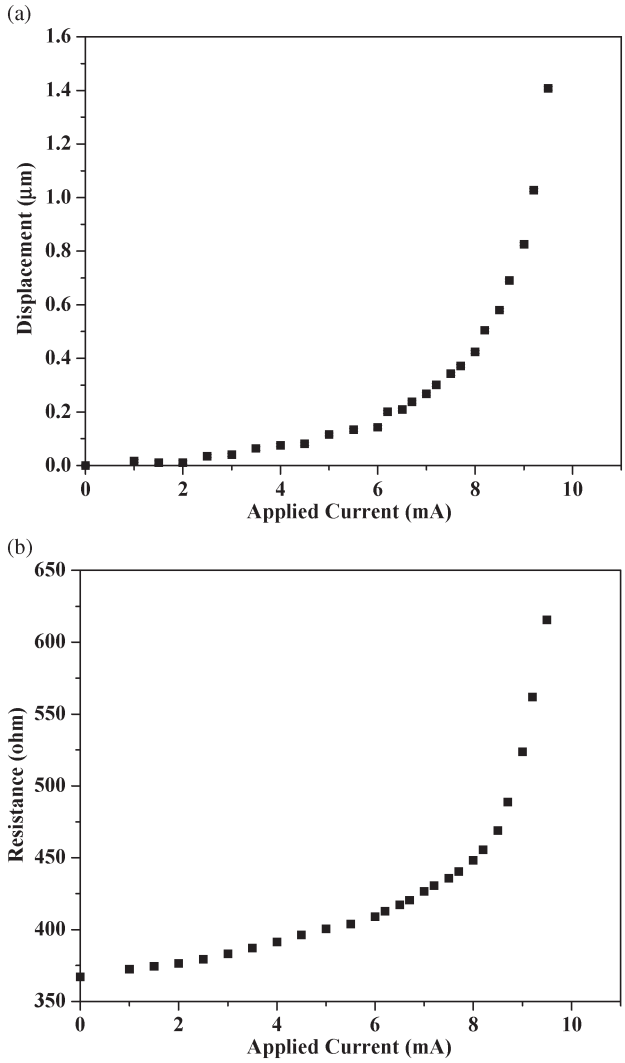

Fig. 2. (a) Displacement and (b) resistance as functions of applied current.

of SCS rises as its temperature increases. Fig. 2(b) shows the resistance change of the ZTA as a function of the applied current (no external force on the ZTA); the resistance change is mainly due to the temperature change in the device. With an external force, the resistance at the given current further changes due to the piezoresistive effect. However, the change in resistivity due to the piezoresistivity is much smaller than that caused by the temperature change. Hence, we assume that the small resistance change caused by the piezoresistive effect has negligible effect on the thermal characteristics, or temperature profile, of the ZTA.

A. Experimental Measurement of Piezoresistivity

To test the resistance change due to the piezoresistive effect only, a given current of the ZTA was maintained constant while an external force was exerted to the ZTA. A tungsten probe (Model 7B-2, Micromanipulator) attached to a nanomanipulator (Klocke Nanotechnik, Aachen, Germany) inside SEM was used to push the ZTA in the opposite direction of its movement. The probe was positioned in the middle of the shuttle (guided by SEM imaging) to prevent in-plane rotation of the ZTA. For each

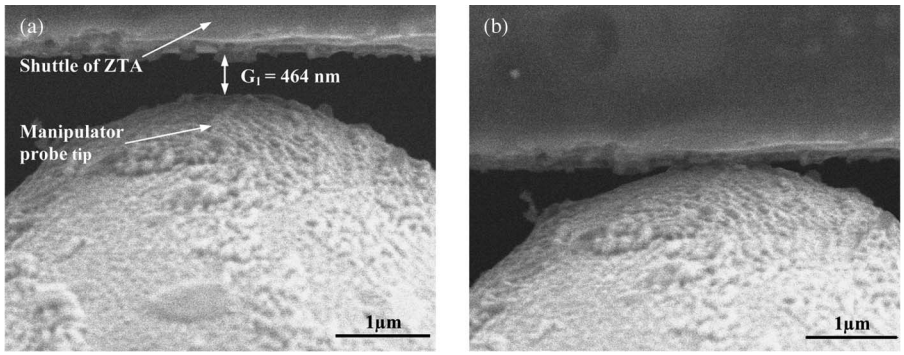

Fig. 3. Experimental process for the piezoresistivity measurement. (a) Gap between the ZTA and the manipulator probe tip is less than D_1 (581 nm at $I_1 = 8.6$ mA) to block the ZTA movement. (b) Probe pushes the ZTA back by 117 nm after I_1 is applied again to the ZTA.

given current and external force, the voltage (thus resistance) and displacement of the ZTA were recorded in the following procedure. Then, different values of current and external force were repeated.

1) The initial position P_0 (i.e., the distance between the shuttle of the ZTA and the tungsten probe, where the tungsten probe served as a reference point) was recorded. The displacement of the ZTA was set as zero. The initial resistance of the ZTA was recorded as R_0.
2) A current (I_1) was applied across the ZTA. The actuated position (P_1) and the output voltage (V_1) were recorded. $D_1 = P_0 - P_1$ is the displacement of the ZTA at current I_1. The resistance (R_1) was calculated by Ohm's law. The resistance change $R_1 - R_0$ is due to the temperature effect.
3) The current was turned off, and the tungsten probe was moved toward the ZTA with a gap G_1 between them (smaller than D_1) [Fig. 3(a)].
4) The same current I_1 was turned on again. The ZTA moved G_1 due to the blocking of the tungsten probe [Fig. 3(b)]. The output voltage (V_2) was recorded to compute the resistance R_2. The resistance change $R_2 - R_1$ is due to the external force exerted by the tungsten probe. Note here that the ZTA displacement was G_1 and the external force was $F = (D_1 - G_1) \times k$, where k is the stiffness of the ZTA. Therefore, the resistance value under a given current and a given external force was obtained. Based on $F = (D_1 - G_1) \times k$, all the force sensing as reported in this paper can be used for displacement sensing.
5) Steps 3) and 4) were repeated with different gaps between the tungsten probe and the ZTA (G_2, G_3, G_4, etc.) at the same current (I_1) to obtain more external forces (and ZTA displacements) for this given current.
6) Steps 2)–5) were repeated with different current levels (I_2, I_3, I_4, etc.) until sufficient data points were acquired.

Two assumptions are made in the aforementioned experiments and data analysis. First, the tungsten probe does not affect the temperature profile of the ZTA at a given current when they are in contact. A ceramic thermal insulator layer is placed between the tungsten probe and the nanomanipulator base. Second, the tungsten probe is treated as a rigid body in view that its stiffness is much larger than that of the ZTA. These assumptions will be checked with finite-element analysis (to be described).

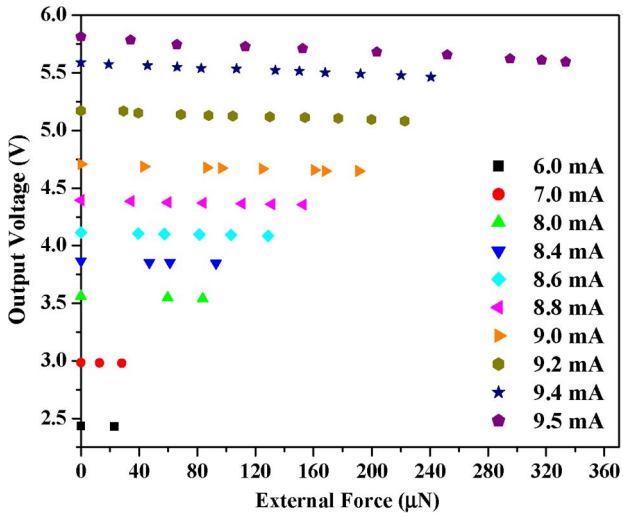

Fig. 4. Voltage versus external force for all current levels. For each current, the external force starts as zero (no applied force) and increases.

B. Experimental Results of Piezoresistivity

All experiments were carried out inside a SEM (JEOL 6400F) under vacuum and room temperature. The displacements and gaps were measured from the SEM images with a resolution of 4.6 nm. The initial resistance (under room temperature) and the stiffness of the ZTA were 367.3 Ω and 274.3 N/m, respectively.

In our experiments, the data were collected for the applied current ranging from 6.0 to 9.5 mA. When the current is smaller than 6.0 mA, the displacement of the ZTA is very small (< 200 nm), which presents a challenge to precisely control the gap between the ZTA and the tungsten probe. On the other hand, if the applied current is very high (e.g., > 10 mA), recrystallization of SCS could occur [19]. Thus, we kept the applied currents less than 10 mA in all our experiments.

The experimental results are shown in Figs. 4–6. Under different current levels, the output voltage (V_2) is plotted as a function of the external force in Fig. 4. In the experiments, the direction of the external force was opposite to the moving direction of the ZTA, which is set as positive. Note that, at the same current level, the resistance (R_2) (obtained from the

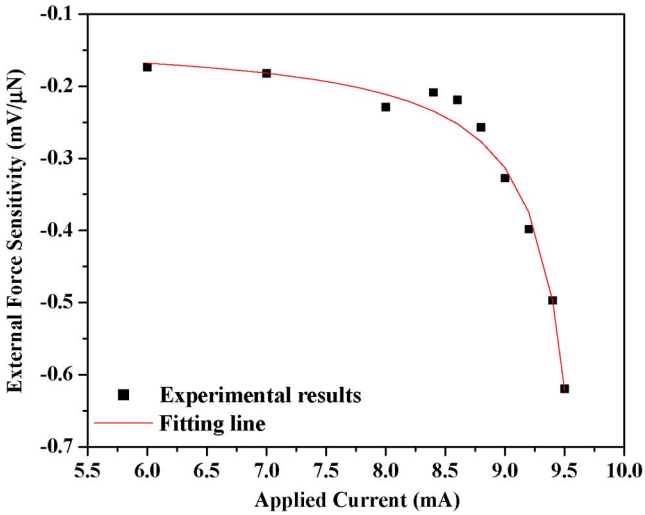

Fig. 5. External force sensitivity at different current levels.

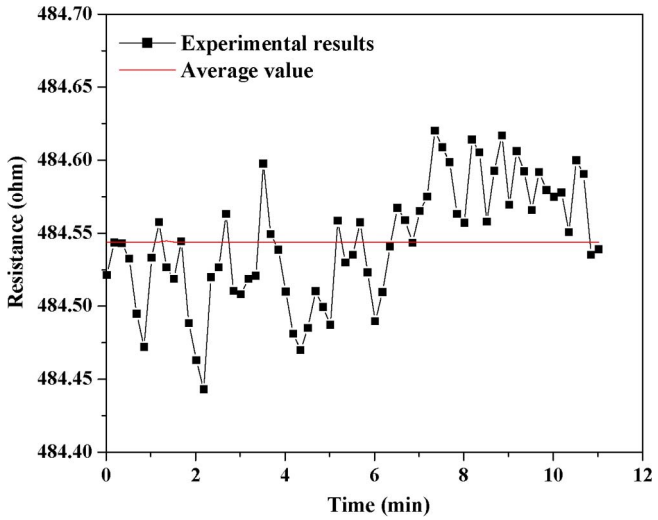

Fig. 6. Noise of the resistance at the applied current of 8.6 mA. The red line is the average value of all the data points.

voltage shown in Fig. 4) decreased with the increase of the external force, due to the piezoresistive effect. As shown in Fig. 4, at 8.6-mA current level, for instance, the output voltage linearly decreased from 4.114 to 4.086 V (i.e., the resistance decreased from 478.4 to 475.1 Ω) when the external force increased from 0 to 128.65 μN. For a given current level, an unloaded ZTA reached its maximum displacement. Applying an external force while maintaining the same current therefore increases the compressive stresses in the beams, which, in turn, induces the decrease in voltage due to the piezoresistive effect. Fig. 4 clearly shows that the ZTA can be used to sense external force by measuring the output voltage.

The sensitivity α, defined as the slope of the linear fitting under each applied current level in Fig. 4, varies with the applied current, as shown in Fig. 5. The negative value of the sensitivity means that, when the external force increases, the output voltage decreases. The sensitivity levels off initially and increases sharply when the current is over 8.6 mA. For example, at the current level of 8.6 mA, when the ZTA is pushed back by an external force of 1 μN, the output voltage and resistance decrease by 0.22 mV and 25.6 mΩ, respectively. The resolution of the force sensor is ultimately determined by the noise level. Fig. 6 shows the resistance fluctuation at 8.6-mA current in 11 min. The noise can be quantified by the root-mean-square deviation of the experimental data, viz.,

$$R_n = \sqrt{\frac{\sum_{i=1}^{N}(R_i - \overline{R})^2}{N}} \tag{1}$$

where R_n is the resistance noise, R_i is the data point, $\overline{R}$ is the average value, and N is the number of the data. The resistance noise was 0.042 Ω at 8.6 mA according to (1). The noise is possibly due to stray electromagnetic fields present inside the chamber, stage vibration, or electron-beam-induced heating. Based upon the measured sensitivity and noise, the resolution of the force sensor is given by $R_n I/|\alpha|$, where I is the applied current. The load resolution of 1.64 μN at 8.6-mA current was obtained. Note that the load resolution can be substantially improved by reducing the stiffness of the ZTA.

TABLE I
DIMENSIONS OF THE ZTA USED IN SIMULATIONS

Dimension	Symbol	Value	Unit
Beam length	L	88	μm
Beam width	W	4	μm
Thickness	t	10	μm
Eccentricity	l	20	μm
Shuttle length	L_S	92	μm
Shuttle width	W_S	60	μm

C. Multiphysics Simulation

To validate the assumptions in the experiments, nonlinear multiphysics simulations using ANSYS 11.0 were performed. The dimensions of the ZTA (the same as those in the experiments) and the material parameters used in the simulations are listed in Tables I and II, respectively. The three piezoresistance coefficients (π_{11}, π_{12}, and π_{44}) are dependent on several factors, including temperature, doping concentration, original bulk resistivity, crystalline structure, and surface concentration of the diffused layer [20], [21]. Some of these factors are difficult to measure or quantify. In our work, these coefficients are approximated from [22] and [23] (see Table II). The element type for the multiphysics simulation in ANSYS is *Solid 226* that is a 3-D element type for both thermal–electric-structural analysis and piezoresistive analysis. A series of simulations was performed at different currents and external forces. Fig. 7(a) and (b) shows the simulated displacement and output voltage of the ZTA before and after it was subjected to an external force of 20 μN, respectively, while the current is maintained at 8.6 mA. When the ZTA is pushed back by 0.071 μm under the 8.6-mA current, the output voltage decreases by 0.005 V. The simulation results agreed very well with those of the experiments, as shown in Fig. 8.

It is important to note that the Z-shaped beams are not under pure bending (i.e., the tensile strain and compressive

TABLE II
MATERIAL PARAMETERS USED IN SIMULATIONS

Parameter	Symbol	Value	Unit
Young's modulus	E	160	GPa
Poisson's ratio	v	0.28	-
Thermal conductivity (constant)	K	146	W/(mK)
Thermal conductivity (temperature dependant)	$K(T)$	$210658 \times T^{-1.2747}$	W/(mK)
Thermal expansion coefficient (constant)	α	2.5×10^{-6}	K^{-1}
Thermal expansion coefficient (temperature dependant)	$\alpha(T)$	$-4 \times 10^{-12}\, T^2 + 8 \times 10^{-9}\, T + 4 \times 10^{-7}$	K^{-1}
Resistivity (constant)	ρ	5.1×10^{-5}	Ωm
Resistivity (temperature dependant)	$\rho(T)$	$5.1 \times 10^{-5}\,[1 + 3 \times 10^{-3}(T - 273)]$	Ωm
Piezoresistance coefficients	π_{11}	-15×10^{-11}	Pa^{-1}
	π_{12}	7.5×10^{-11}	Pa^{-1}
	π_{44}	-12×10^{-11}	Pa^{-1}

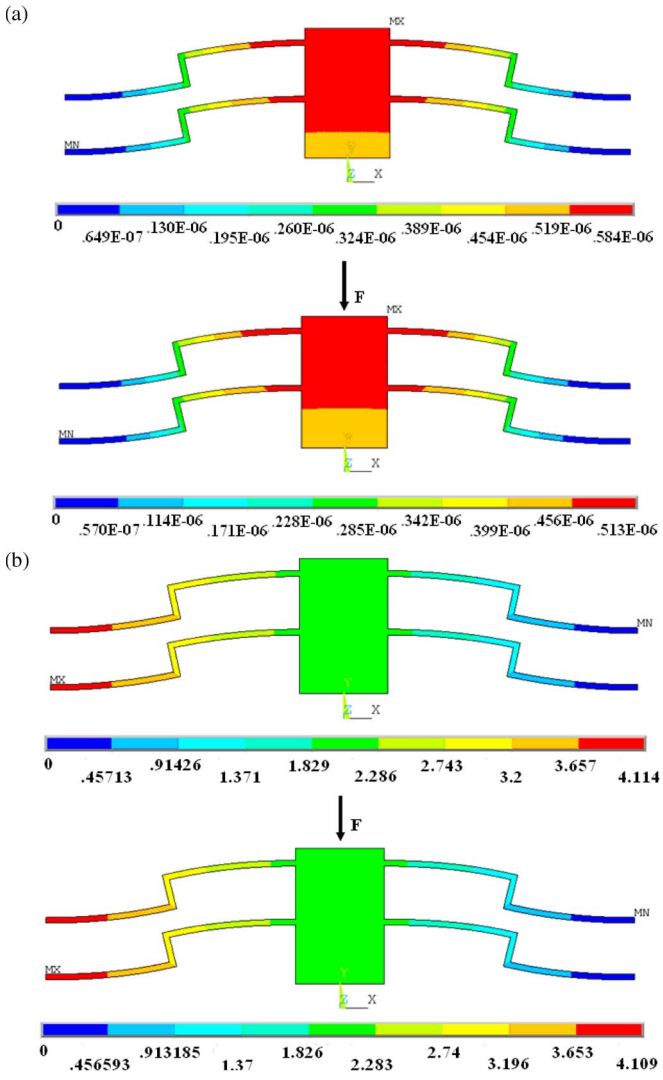

Fig. 7. Simulation results at the 8.6-mA current level with the external force of 20 μN. (a) Displacement of the shuttle changes from 0.584 to 0.513 μm. (b) Output voltage changes from 4.114 to 4.109 V.

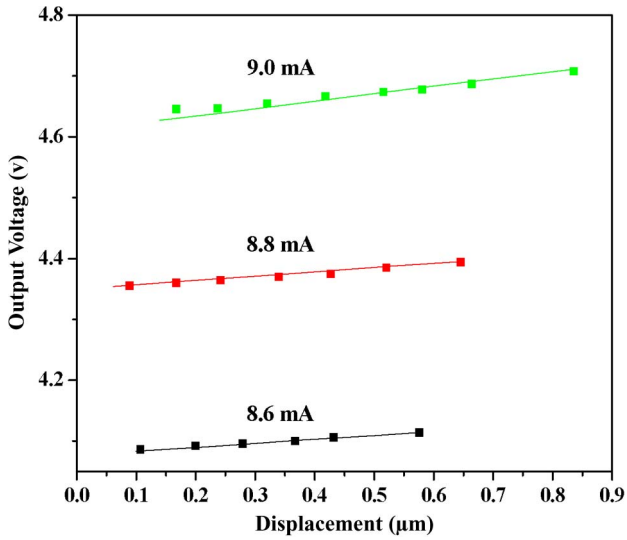

Fig. 8. Comparison between the simulated and experimental results at 8.6-, 8.8-, and 9.0-mA current levels. Dots and lines represent the experimental and simulated results, respectively. In the multiphysics simulations, temperature-dependent resistivity and thermal expansion coefficient were used (see Table II).

strain on either side of the beam do not cancel out). Instead, an overall compression exists in the Z-shaped beams, which is believed to be responsible for the piezoresistive response. Similar piezoresistive responses have been observed for V-shaped thermal actuators [16].

IV. FEEDBACK CONTROL SYSTEM

In this section, a feedback control system based on the piezoresistive sensing characteristics of the ZTA is demonstrated. The function of this feedback control system is that, when the ZTA is pushed by an external force, the feedback system actively updates the current input to compensate the ZTA displacement to the value without the external force (i.e., bring the ZTA to its initial position), while measuring the external force simultaneously.

A. Data Fitting of the Piezoresistivity Measurements

The ZTA response can be viewed to have two inputs and two outputs; the two inputs are electric current (I) and external force (F), and the two outputs are displacement (D)

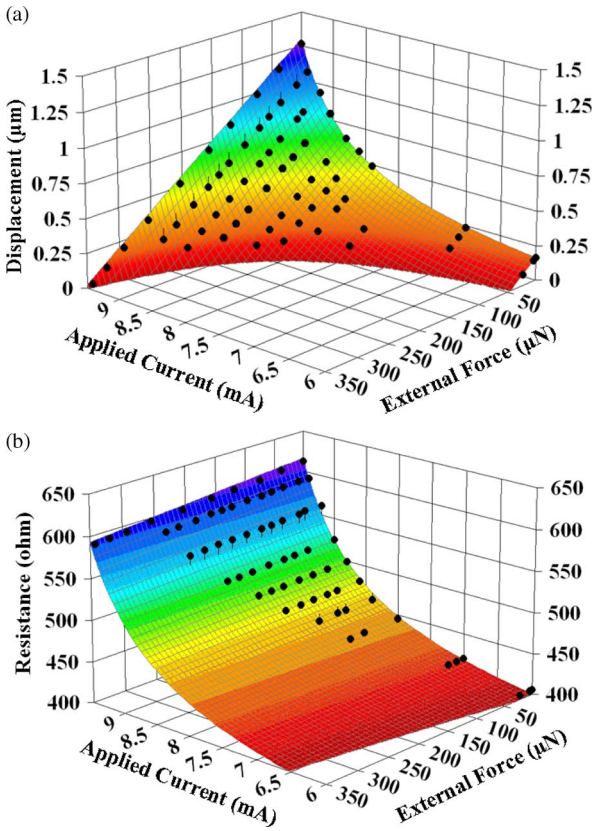

Fig. 9. (a) Displacement as a function of the applied current and external force. (b) Resistance as a function of the applied current and external force.

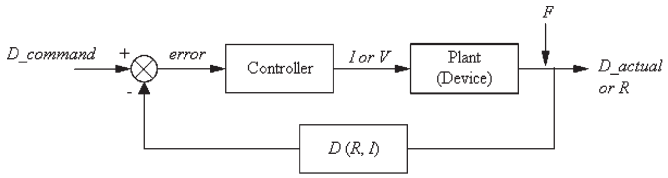

Fig. 10. Feedback control system with compensator block diagram.

and electric resistance (R) (or voltage V). A key step is to identify two fitting functions. Fig. 9 shows the fittings for both outputs (displacement and resistance) as functions of the inputs (current and external force). First of all, the displacement and resistance (when external force is zero) are fitted as functions of the current alone. The best functions that we identified are given by

$$D|_{F=0} = \frac{0.14I}{-1.22I + 12.55} \tag{2a}$$

$$R|_{F=0} = \frac{-32.77I + 367.26}{-0.096I + 1}. \tag{2b}$$

Several material properties, such as thermal conductivity, thermal expansion coefficient, and resistivity, are typically temperature dependent (see Table II). This fact determines the types of fit (rational), numerator (linear polynomial), and denominator (linear polynomial). Note that the contribution of the current to both the displacement and resistance is independent of the external force. When considering the contribution of

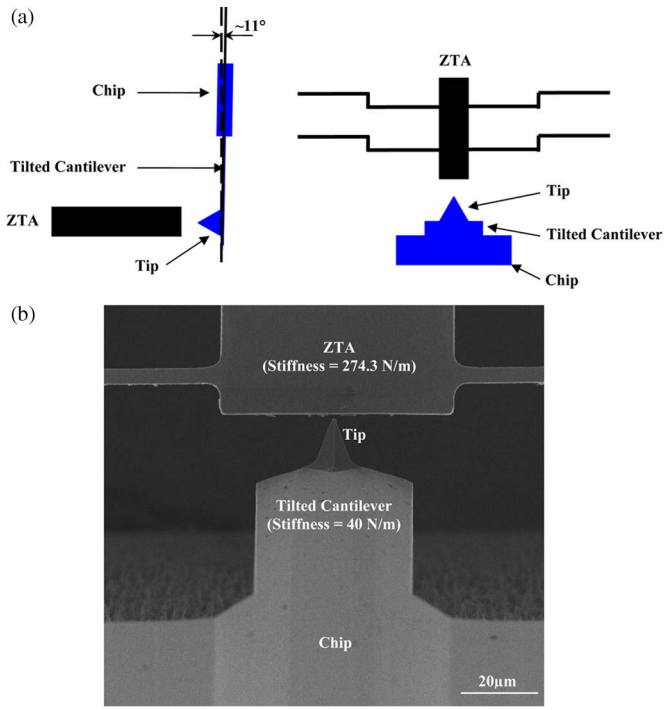

Fig. 11. Overview of the closed-loop feedback experiment. The AFM cantilever is oriented perpendicular to the ZTA and parallel to the electron beam. The AFM tip is used to push the ZTA. (a) Schematic showing the position of the ZTA and cantilever. Left shows side view, and right shows top view. An 11° tilt of the AFM cantilever is used to ensure a clear observation of the setup. (b) SEM image showing the overview of the closed-loop feedback setup inside SEM chamber.

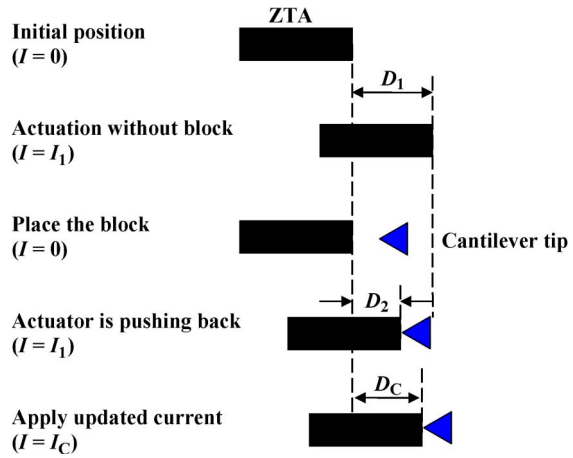

Fig. 12. Feedback control experiment to maintain a constant position of the ZTA. Ideally, D_C equals D_1.

the external force, the displacement and resistance are best fitted by

$$D(I,F) = \frac{0.14I}{-1.22I + 12.55} - \frac{F}{274.3} \tag{3a}$$

$$R(I,F) = \frac{-32.77I + 367.26}{-0.096I + 1} - \frac{-0.21I + 2.37}{-1.86I + 18.29}\frac{F}{I}. \tag{3b}$$

The displacement depends on the external force simply following Hooke's law with the stiffness of the ZTA equal to 274.3 N/m. Such dependence does not change with the current. The resistance also depends on the external force due to the

TABLE III
COMPARISON OF INITIAL CURRENT AND FINAL UPDATED CURRENT UNDER DIFFERENT EXTERNAL FORCES APPLIED FOR FEEDBACK EXPERIMENT, AND THE CALCULATED ERROR COEFFICIENT ε

Initial Current (mA)	Initial External Force (μN)	Final Updated Current (mA)	Error Coefficient (%)
8	45.53	8.56	8.19
8	99.74	8.94	3.87
8.5	75.84	9.03	14.6
8.5	109.92	9.17	9.76
9	120.281	9.41	2.42
9	178.175	9.53	6.3
9.3	113.01	9.56	0.1
9.3	127.165	9.575	9.62
9.3	226.29	9.703	6.21
9.5	98.91	9.65	1.38
9.5	323.104	9.85	4.89
9.5	355.137	9.87	3.96

piezoresistive effect. The piezoresistive effect is dependent on the current. As shown in Fig. 5, the sensitivity (i.e. the slope of the data points at each current level in Fig. 4) changes with the current. This is why the second term in (3b) involves the current.

The accuracy of the aforementioned fitting functions was evaluated by the coefficient of determination, which is defined as

$$R^2 = 1 - \frac{SS_{\text{err}}}{SS_{\text{tot}}}, \qquad R^2 \in [0, 1] \tag{4}$$

where $SS_{\text{err}} = \sum_{i=1}^{n}(z_i - \hat{z}_i)^2$ and $SS_{\text{tot}} = \sum_{i=1}^{n}(z_i - \bar{z}_i)^2$ (n represents the number of data points, z_i represents the measured data, $\hat{z}_i$ represents the fitted data, and $\bar{z}_i$ represents the mean of the measured data). The coefficients of determination for (2a), (2b), (3a), and (3b) were 0.993, 0.994, 0.991, and 0.991, respectively, which indicated that excellent fittings were indeed obtained.

B. Design of Feedback Control System

A feedback control system was built based on the calibrated relationships, as shown in (3). The objective of the feedback system was to, for a given current, maintain the constant displacement under various external forces under quasi-static loading. Here, the desired displacement is the set point (for simplicity, when the external force is zero), the sensed resistance is the process variable, the current is the manipulated variable, and the external force is the disturbance. The block diagram of the feedback system is shown in Fig. 10. The controller was built in LabVIEW (version 8.5, National Instruments) with a nonlinear algorithm given as

$$\frac{0.14I}{-1.22I + 12.55} + e = \frac{0.14I_0}{-1.22I_0 + 12.55} \tag{5}$$

where I is the updated current, I_0 is the initial current, and $e\ (= -(F/274.3))$ is the error between the initial displacement and sensed displacement, as shown in Fig. 10. The signals of output voltage and updated current were read and written by the computer through a multifunction data acquisition module (DAQ NI USB-6211, National Instruments). The LabVIEW controller works as follows: When an output voltage is read in from the ZTA, the controller converts it to a resistance value based on the given current and then computes the external force and the sensed displacement according to (3b) and (3a), respectively. The updated current to maintain the displacement is computed by (5). The data acquisition module can only read/write voltage signals; hence, a simple circuit was built to convert voltage signals to current signals and vice versa.

C. Experimental Results of Feedback Control

In the feedback control experiments, the stiffness of the blocking object (applying the external force) cannot be infinite as the tungsten probe that is used in the piezoresistivity measurements. Consequently, an atomic force microscope (AFM) cantilever (Model ACTA, Nanoscience Instruments) with a stiffness of 40 N/m was used. The AFM cantilever was oriented perpendicular to the ZTA and parallel to the electron beam, as shown in Fig. 11(a). An overview of the experimental setup inside SEM is shown in Fig. 11(b). The feedback control system experiments were also carried out inside the SEM chamber, with the same experimental conditions as in the piezoresistivity experiments. The experimental process is shown schematically in Fig. 12. Initially, the process was the same as the piezoresistivity experiment from step 1) to step 4). Then, the output voltage was read into the computer through the input port of the data acquisition module. How much updated current should be applied to generate the corresponding displacement for counteracting the external force was calculated by the LabVIEW program in real time. Finally, the updated current was written out to the ZTA through the output port of the data acquisition module. However, when the updated current was applied to the system, the external force changed as a result. Therefore, the LabVIEW program iterated the comparison between the present position and initial position. The current was updated repeatedly until the ZTA moved back to its initial position.

The performance of the feedback control system under different current levels (from 8.0 to 9.5 mA) was tested. Table III lists all the initial currents, the measured initial external forces (using the feedback system), and the final updated currents. The displacements of the ZTA after applying the updated current were compared with the case of no external force (AFM cantilever). The actuator movements were independently measured

by SEM images. To evaluate the accuracy of the feedback system, an error coefficient ε is introduced as follows:

$$\varepsilon = \frac{|D_C - D_1|}{D_1 - D_2} \times 100\% \tag{6}$$

where D_C is the displacement of the ZTA after applying the updated current with the presence of the AFM cantilever, D_1 is the displacement of the ZTA without the external force, and D_2 is the displacement with the external force (as shown in Fig. 12). The smaller the ε, the better the feedback accuracy. $\varepsilon = 0$ means that the ZTA is moved back to the initial position.

ε as a function of the external force at different current levels is also listed in Table III. It is seen that ε is smaller than 10% in nearly all cases (except one case), which indicates that the feedback system works quite well. It appears that ε increases as the external force decreases. The main error sources include resistance measurement (noise and drift), displacement measurement using SEM, and data fitting. Wheatstone bridge [13], [24] is a common method to improve the performance in resistance measurement. Our future work includes designing identical thermal actuators and implementing the Wheatstone bridge method. We emphasize that the feedback system developed in the present work is only for quasi-static loading. A PID controller will be integrated to the existing setup to improve the dynamic response.

V. Conclusion

This paper has reported the piezoresistive response and preliminary results for feedback control of ZTAs. We characterized the piezoresistive response of ZTAs by *in situ* SEM nanomanipulation and demonstrated ZTAs as viable piezoresistive sensors. We found that their sensitivity depends on the applied current and is ultimately limited by the noise. The piezoresistive response was simulated by ANSYS multiphysics, which gave excellent agreement with the experiments. We further treated the ZTA as a two-input (applied current and external force) and two-output (displacement and electric resistance) system. Based on the modeled relationships between the inputs and the outputs, we developed a feedback system that can simultaneously sense the external force and generate updated current to actuate the ZTA to the desired position. We demonstrated this feedback control by holding the ZTA at a constant position under various external forces under quasi-static loading. The feedback system worked quite well with errors less than 10% for almost all the experiments. Such a feedback control is valuable for a range of MEMS applications, including on-chip nanoscale mechanical testing and nanopositioning. As an example, for nanoscale mechanical testing, the feedback scheme is expected to make possible true displacement control, which is critical in capturing some advanced mechanical properties such as phase transformation, strain softening, and stress relaxation.

Acknowledgment

The authors would like to thank Prof. J. Dong for the valuable discussion on the feedback control and Q. Qin for the assistance with the *in situ* scanning electron microscope (SEM) experiments. The *in situ* SEM experiments were performed in the Analytical Instrumentation Facility at North Carolina State University. The authors would also like to thank both anonymous reviewers for the valuable comments and suggestions.

References

[1] Q.-A. Huang and N. K. S. Lee, "Analysis and design of polysilicon thermal flexure actuator," *J. Micromech. Microeng.*, vol. 9, no. 1, pp. 64–70, Mar. 1999.

[2] C. Guan and Y. Zhu, "An electrothermal microactuator with Z-shaped beams," *J. Micromech. Microeng.*, vol. 20, no. 8, pp. 085014-1–085014-9, Aug. 2010.

[3] R. Cragun and L. L. Howell, "Linear thermomechanical microactuators," in *Proc. ASME Int. Mech. Eng. Congr. Expo., MEMS*, Nov. 1999, pp. 181–188.

[4] L. Que, J.-S. Park, and Y. B. Gianchandani, "Bent-beam electrothermal actuators—Part I: Single beam and cascaded devices," *J. Microelectromech. Syst.*, vol. 10, no. 2, pp. 247–254, Jun. 2001.

[5] R. Hickey, D. Sameoto, T. Hubbard, and M. Kujath, "Time and frequency response of two-arm micromachined thermal actuators," *J. Micromech. Microeng.*, vol. 13, no. 1, pp. 40–46, Jan. 2003.

[6] Y. Zhu, A. Corigliano, and H. D. Espinosa, "A thermal actuator for nanoscale in situ microscopy testing: Design and characterization," *J. Micromech. Microeng.*, vol. 16, no. 2, pp. 242–253, Feb. 2006.

[7] Y. Zhu and H. D. Espinosa, "An electromechanical material testing system for in situ electron microscopy and applications," *Proc. Nat. Acad. Sci.*, vol. 102, no. 41, pp. 14 503–14 508, Oct. 2005.

[8] Y. Zhu, N. Moldovan, and H. D. Espinosa, "A microelectromechanical load sensor for in situ electron and X-ray microscopy tensile testing of nanostructures," *Appl. Phys. Lett.*, vol. 86, no. 1, pp. 013506-1–013506-3, Jan. 2005.

[9] J.-S. Park, L. L. Chu, A. D. Oliver, and Y. B. Gianchandani, "Bent-beam electrothermal actuators—Part II: Linear and rotary microengines," *J. Microelectromech. Syst.*, vol. 10, no. 2, pp. 255–262, Jun. 2001.

[10] L. L. Chu and Y. B. Gianchandani, "A micromachined 2D positioner with electrothermal actuation and sub-nanometer capacitive sensing," *J. Micromech. Microeng.*, vol. 13, no. 2, pp. 279–285, Mar. 2003.

[11] M. S. Baker and L. L. Howell, "On-chip actuator of an in-plane compliant bistable micromechanism," *J. Microelectromech. Syst.*, vol. 11, no. 5, pp. 566–573, Oct. 2002.

[12] J. Dong and P. M. Ferreira, "Simultaneous actuation and displacement sensing for electrostatic drives," *J. Micromech. Microeng.*, vol. 18, no. 3, pp. 035011-1–035011-1, Jan. 2008.

[13] R. K. Messenger, Q. T. Aten, T. W. McLain, and L. L. Howell, "Piezoresistive feedback control of a MEMS thermal actuator," *J. Microelectromech. Syst.*, vol. 18, no. 6, pp. 1267–1278, Dec. 2009.

[14] H. D. Espinosa, Y. Zhu, and N. Moldovan, "Design and operation of a MEMS-based material testing system for nanomechanical characterization," *J. Microelectromech. Syst.*, vol. 16, no. 5, pp. 1219–1231, Oct. 2007.

[15] S. D. Senturia, *Microsystem Design*. Boston, MA: Kluwer, 2001.

[16] T. L. Waterfall, K. B. Teichert, and B. D. Jensen, "Simultaneous on-chip sensing and actuation using the thermomechanical in-plane microactuator," *J. Microelectromech. Syst.*, vol. 17, no. 5, pp. 1204–1209, Oct. 2008.

[17] K. Kim, X. Liu, Y. Zhang, and Y. Sun, "Nanonewton force-controlled manipulation of biological cells using a monolithic MEMS microgripper with two-axis force feedback," *J. Micromech. Microeng.*, vol. 18, pp. 055013-1–055013-8, May 2008.

[18] A. Cowen, G. Hams, D. Monk, S. Wilcenski, and B. Hardy, *SOIMUMPs Design Handbook*. Bernin, France: MEMSCAP. [Online]. Available: http://www.memscap.com/mumps/documents/SOIMUMPs.dr.v4.pdf

[19] M. Chiao and L. Lin, "Self-buckling of micromachined beams under resistive heating," *J. Microelectromech. Syst.*, vol. 9, no. 1, pp. 146–151, Mar. 2000.

[20] C. Liu, *Foundations of MEMS*. Upper Saddle River, NJ: Pearson, 2006.

[21] G. K. Johns, L. L. Howell, B. D. Jensen, and T. W. McLain, "A model for predicting the piezoresistive effect in microflexures experiencing bending and tension loads," *J. Microelectromech. Syst.*, vol. 17, no. 1, pp. 226–235, Feb. 2008.

[22] O. N. Tufte and E. L. Stelzer, "Piezoresistive properties of silicon diffused layers," *J. Appl. Phys.*, vol. 34, no. 2, pp. 313–318, Feb. 1963.

[23] Y. Kanda, "Piezoresistance effect of silicon," *Sens. Actuators A, Phys.*, vol. 28, no. 2, pp. 83–91, Jul. 1991.

[24] A. A. Barlian, W.-T. Park, J. J. R. Mallon, A. J. Rastegar, and B. L. Pruitt, "Review: Semiconductor piezoresistance for microsystems," *Proc. IEEE*, vol. 97, no. 3, pp. 513–552, Mar. 2009.

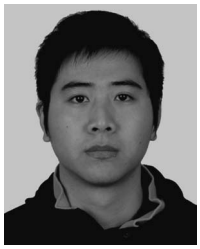

Jing Ouyang received the B.E. degree in mechanical and electrical engineering from Central South University, Changsha, China, in 2009, and the M.S. degree in mechanical engineering from North Carolina State University, Raleigh, in 2011.

He is currently with the Department of Mechanical and Aerospace Engineering, North Carolina State University. His graduate research focused mainly on microelectromechanical systems, particularly on the piezoresistive effect of microdevices.

Yong Zhu received the B.S. degree in mechanical engineering from the University of Science and Technology of China, Hefei, China, in 1999, and the M.S. and Ph.D. degrees in mechanical engineering from Northwestern University, Evanston, IL, in 2001 and 2005, respectively.

Since 2007, he has been with North Carolina State University, Raleigh, where he is currently an Assistant Professor in the Department of Mechanical and Aerospace Engineering. His research interests lie at the interface between micro-/nanotechnology and mechanics of materials, including mechanics and electromechanical coupling of nanostructures, micro-/nanoelectromechanical systems, stretchable nanodevices for energy and biomedical applications, and adhesion/friction at the nanoscale.